Chapter

Laser Floating Zone: General Overview Focusing on the Oxyorthosilicates Growth

Francisco Rey-García, Carmen Bao-Varela and Florinda M. Costa

Abstract

This chapter reviews the laser floating zone (LFZ) technique, also known as the laser-heated pedestal growth (LHPG), focusing on the recently produced rare-earth-doped oxyorthosilicate fibers. LFZ has been revealed as a suitable prototyping technique since high-quality crystals can be developed in short time with low consumption of precursor materials in a crucible-free processing that ensures to practically avoid by-products. Moreover, additional advantages are the possibility to treat and melt highly refractory materials together with the easy way for tailoring the final microstructural characteristics and this way the macroscopic physical properties. Thus, refractory rare-earth (RE) doped oxyorthosilicates following the formula RE_2SiO_5 have been recently produced by the LFZ technique for tuning laser emission parameters. The oxyorthosilicates have high chemical stability and allow incorporation of many rare-earth ions yielding different applications, such as laser host materials, gamma ray detectors or scintillators, environmental barrier coatings (EBCs) and waveguides, among others. Thus, different kinds of oxyorthosilicates were produced by the LFZ technique, and the detailed effects of the main processing parameters on crystal's characteristics are discussed in this chapter.

Keywords: laser floating zone, crystal growth, oxyorthosilicates, rare earths, single crystal, polycrystalline ceramics

1. Introduction

The production of high-quality silicate-based single crystals is mainly accomplished by solid state and Czochralski methods ([1–9] and references therein). However, these methods require several amounts of material and the use of crucibles that can introduce external contamination. Moreover, expensive crucibles such as platinum or iridium and special atmospheres are usually necessary when the desired materials are refractory or their chemical reactivity can negatively affect the phase development. So, all these restrictions together with long processing time considerably increase the production costs, being not the most suitable approach for materials prototyping.

The micro-pulling down (μPD) and the floating zone (FZ) are alternative techniques to grow crystalline fibers from a melt [10–12]. The μPD technique is suitable for prototyping; however, the melt is continuously in contact with crucible, being

also applied low pulling rates. Concerning the FZ technique, the preform materials with cylindrical geometry (rods) are placed inside a mirror-like concave chamber provided with halogen lamps that allow the material melting in a small region. These techniques are complex and limited by the melting point of the materials.

The laser floating zone (LFZ) technique is similar to the FZ; however, a laser beam, guided into a closed chamber through a ZnSe window, is used to melt the top of a feed rod precursor material. Afterwards, a seed rod is immersed into the molten zone and pulled at a controlled pulling rate [13, 14]. This technique presents many advantages when compared with standard growth methods, namely the growth at high pulling rates, the synthesis of materials with very high melting temperature [15–17] and the most important one: it is a crucible-free process, thus avoiding any external related contamination [14, 18]. This way high purity crystals can be obtained in a short time from a small amount of raw material and minor energy consumption. Moreover, being a nonequilibrium process, metastable phases can be developed from the solid/liquid interface due to the very high thermal gradients [19]. **Figure 1** puts in evidence a scheme of the LFZ process.

The LFZ equipment comprises a laser system coupled to a reflective optical setup, composed by a *reflaxicon*, and a plane mirror and a parabolic mirror. The term *reflaxicon* was introduced in 1970 by Edmonds [20], and it describes a two-stage pair of reflective linear axicon surfaces (**Figures 1** and **2**). As Edmonds [20] did not consider nonlinear axicons, all the applications that he proposed were afocal in nature. This reflective device essentially consists of a primary conical mirror and a larger secondary conical mirror coaxially located with respect to the primary. The function of this device is to convert a solid light beam into a hollow one in an essentially lossless manner (except for absorption at the mirror surface and other similar phenomena). This device is similar to the one patented by Martin in 1948 [21]. A circular crown-shaped laser beam is obtained by the mirror aiming to produce a uniform radial heating. In the LFZ process, after the *reflaxicon*, the plane mirror setted up 45° allows the laser beam reflection to the vertical position in the direction of the spherical or parabolic mirror. The rod precursor defines the crown size of the fiber produced, and a floating zone configuration is obtained [14, 18]. It must be noted that mirrors have a hole in their centers allowing feed and seed holders be placed in the optical axis [14]. Furthermore, the use of a closed chamber allows the growth under controlled atmosphere [22]. Additionally, the growth is controlled by a camera video system focused into the floating zone area allowing to observe the molten zone and particularly the melting and the crystallization interface [18].

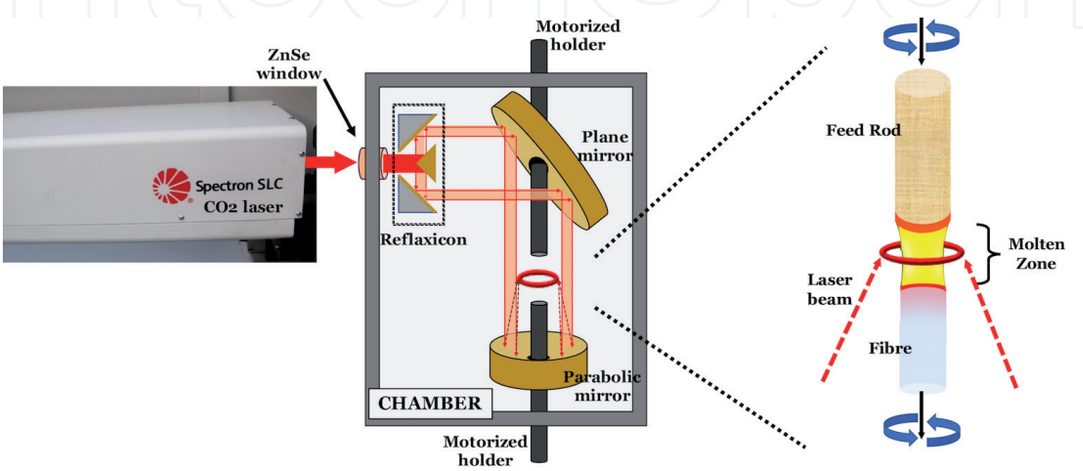

Figure 1.
Laser floating zone setup, highlighting the molten zone.

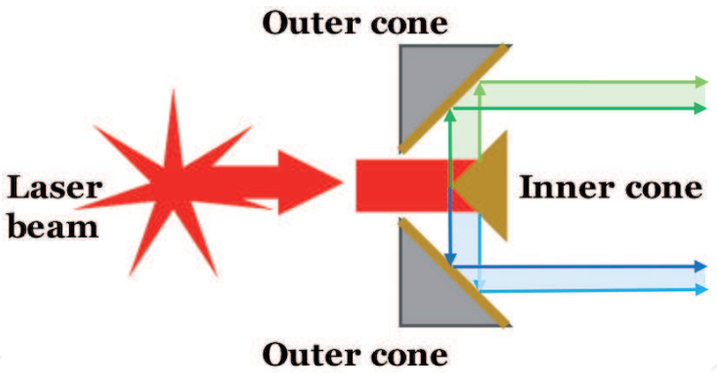

Figure 2.
Reflaxicon *performance noting light guiding with different colors to enhance comprehension.*

Andreeta et al. [14] have reported a good description of the LFZ systems, putting in evidence their modifications of the LFZ systems over the years. A highlight is made to all processes developed to control/modify the temperature gradient at the solid/liquid interface localized between the molten zone and feed/seed rods (**Figure 1**). Noteworthy is the method of electrically assisted laser floating zone (EALFZ) [23, 24] that explores a new mechanism for controlling the solidification process by applying an electric current through the solid/liquid interface. In the presence of an electric current, the solute transport depends not only on the local solute gradient but also on the electromigration of solute that will modify the composition and the characteristic length scale of the solute diffusion field ahead of crystals. The application of an electrical current strongly modified phase development, crystal shapes and effective distribution coefficients. The enhancement of nucleation rate and of the driving force for ion migration along the fiber axis promotes a strong increase in the grain alignment and consequently on the physical properties [25, 26].

The LFZ method enables the development of high-quality light emitting materials and transparent conductive oxides with rare-earth doping [15, 27, 28] along with the growth of complex ceramic materials such as thermoelectric oxide materials [25, 29], high-temperature ceramic superconductors [19, 23, 26] and eutectic oxides [13, 30]. Alongside, by controlling the laser irradiance and the pulling rate, it is possible to determine the crystallization kinetics aiming to obtain highly oriented single or polycrystalline materials, with enhanced physical properties [16, 19, 24].

2. Oxyorthosilicates

Considering the LFZ characteristics, the focus of this work is on oxyorthosilicates, following the formula RE_2SiO_5 (RE = Gd, Lu and Nd). These silicates are highly refractory materials, and despite they present high chemical stability, it is possible to incorporate high concentrations of rare earth ions. Thus, they have attracted the attention of the researchers for long time, yielding different applications [2, 31]. Indeed, since their discovery by Toropov et al. [32], they have been applied as laser host materials [1–3, 9, 33–35], gamma ray detectors or scintillators [36], environmental barrier coatings (EBCs) [37] or, even, as waveguides [38]. The interest in this kind of compounds arose after the first study carried out by Hopkins et al. [39] based on the growth of the rare earth oxyapatites. However, it is important to highlight that these high refractory silicates were grown by the CZ method [1–5, 35–37, 39–41]. For example, Ryba-Romanovski et al. [1] developed solid state yellow lasers based on $(Lu_xGd_{1-x})_2SiO_5$:Sm crystals by CZ, while Wu et al. [41] have

recently grown Cu co-doped Ce:Lu_2SiO_5 crystals at 1.5 mm h^{-1} using a iridium crucible under nitrogen atmosphere for application as scintillators. Furthermore, other approaches for oxyorthosilicates production have been employed during the last years using different methods, like pulsed laser deposition [42], sol–gel [43] or solid-state diffusional process [44]. On the other hand, their production by the LFZ technique is more recent [18, 45–47]; besides, there are two experiments performed in the 1980s decade by de la Fuente et al. [33] and Black et al. [34], who produced $GdNdSiO_5$ and $7Gd_2O_3$•$9SiO_2$:Nd materials applying a high laser power (~185 W).

Aiming to develop new laser materials, Rey-García et al. [18, 46, 47] have recently produced a sort of gadolinium-lutetium oxyorthosilicate materials at low laser powers (<100 W) and pulling rates two to three times faster than those used by Czochralski or other standard methods (1-3 mm h^{-1}). Thus, transparent fibers of Gd_2SiO_5 [18], $(Gd_{0.3}Lu_{0.7})_2SiO_5$ [46] and 5 mol% Y^{3+}:$(Gd_{0.3}Lu_{0.7})_2SiO_5$ [47] have been obtained at 10 mm h^{-1} in air under atmospheric pressure presenting high crystallinity degree. These single crystals present excellent photonic properties that make them useful to be employed as laser host materials due to the Gd^{3+} charger transfer band (CTB) that favors the transfer processes with $4f^7$ transitions from the $^8S_{7/2}$ ground state to energy levels of the dopant element [48–50]. Regarding compositional aspects, despite the similarity observed in these single crystals produced by LFZ, the growing processes based on stoichiometric mixtures of Lu_2O_3 or Nd_2O_3 with SiO_2 bring considerable deviations on the phases diagram associated to crystallization paths that can induce materials evaporation or phases rearrangement [45]. Likewise, the LFZ suitability could be sometimes compromised by precursor's properties, nominal compositions or growing conditions. Consequently, remarkable crack formation can be developed due to internal stress mainly induced by the biaxial character of these silicates and the experimental growing parameters [18].

Summarizing, this chapter will highlight the suitability of the LFZ technique on developing compact and miniaturized crystals envisaging new photonic devices, through the production of low volume bulks with an appropriate geometry based on oxyorthosilicates. The optical fundaments of the LFZ technique together with practical aspects relating to oxyorthosilicates production will be described before showing the microstructural and photonic properties of the materials produced. The idea is to demonstrate the LFZ technique as a suitable, time-saving and economic process for laser materials prototyping compared with traditional techniques [14, 40].

3. Experimental

The extrusion process is the most common way to prepare the precursor rod cylinders for the LFZ process, since it is a simple method, not requiring special equipment or additional hands. Thus, the commercial raw oxide powders are mixed, according to the desired stoichiometry, and reduced into grain size with an agate ball mill for 2 hours at 200 rpm. The purity of the precursors depends on the desired application, being used, in this study, powders of 5–6 N of purity since photonics applications are envisaging. Aiming to bind the powder mixture for extrusion process, polyvinyl alcohol (PVA, 0.1 g ml^{-1}) is added in mashing the powders until a compact and plastic paste is achieved. Then, the obtained clay is extruded into cylindrical rods, with diameters depending on the material applications. In the case of the oxyorthosilicates, diameters ranging 1.5–2.0 mm were selected.

After extrusion, the cylindrical rods are dried in air, being ready to be used as feed and seed materials. However, in the LFZ process, single crystals can also be used as the seed rods [14], favoring the formation of a single crystalline fiber. This approach helps laser processing and allows enhancing the structural

Nominal formula	Sample acronym	Power (W)	Obtained composition	Fiber type
Gd_2SiO_5	GSO	72	Gd_2SiO_5	Crystal
$(Lu_{0.1}Gd_{0.9})_2SiO_5$	LGSO-1	67	$(Lu_{0.12}Gd_{0.88})_2SiO_5$	Crystal
$(Lu_{0.3}Gd_{0.7})_2SiO_5$	LGSO-3	58	$(Lu_{0.31}Gd_{0.69})_2SiO_5$	Crystal
$(Lu_{0.5}Gd_{0.5})_2SiO_5$	LGSO-5	64	$(Lu_{0.53}Gd_{0.47})_2SiO_5$	Crystal
Lu_2SiO_5	LSO-10	92	$Lu_2SiO_5/Lu2O_3$	Eutectics
Nd_2SiO_5	NSO-10	69	$Nd_2SiO_5/Nd_{9.33}(SiO_4)_6O_2$	Biphasic

All fibers have diameters of 1.5 mm for all samples except Lu_2SiO_5 that have 2 mm.

Table 1.
Oxyorthosilicates fibers grown at 10 mm h^{-1} in air by LFZ.

characteristics of the single crystal fiber produced. However, this approach was declined for oxyorthosilicates due to their high melting points.

The LFZ equipment employed for the oxyorthosilicates growth comprise a 200 W CO_2 laser (Spectron, GSI group) coupled to a reflective optical set-up described in the previous section, Optical Fundaments. Once seed and feed fibers are placed on the respective holders, a fast growth process was performed aiming to obtain dense precursor materials. This densification step occurred at 100 mm h^{-1} pulling rate and promotes the PVA decomposition, the formation of the desired phases and enhances the rods mechanical properties. A molten zone is formed by irradiating the densified rods with the CO_2 laser. The fibers were grown in descendent direction from this molten region at 10 mm h^{-1} in air at atmospheric pressure, (crystallization step). Simultaneously during growth, the feed and seed rods rotated at 5 rpm in opposite direction. This procedure favors the mixing of precursors in the melt, homogenizes the temperature of the molten material and contributes to reduce the thermal stresses. In the case of oxyorthosilicate single crystals based on $(Lu_xGd_{1-x})_2SiO_5$ (x = 0–1), the growing process should end by reducing the laser power gradually. This procedure is very important to reduce the thermal stresses and, therefore, avoiding the crack formation.

Table 1 summarizes the experimental conditions to grow oxyorthosilicate fibers at 10 mm h^{-1} in air by LFZ. Considering the Gd_2O_3, Lu_2O_3 and Nd_2O_3 melting points, (2420, 2490 and 2233°C, respectively), the slight variation of the laser power irradiance well matches with this small melting point variation. Despite the experimental conditions are similar, the fibers developed varied from single crystal (GSO and derived silicates) to eutectic (LSO derived) and biphasic (NSO derived) ceramics due to specific characteristic of each phase diagram. Concomitantly, the most remarkable characteristics of the oxyorthosilicates produced in air by LFZ will be described below.

4. Results

Regarding structural properties, the silicates having the formula RE_2SiO_5 are all monoclinic, presenting $P2_1/c$ (Gd_2SiO_5, [18]) or C2/c (Lu_2SiO_5, [45]) space groups depending on the rare earth ions present (**Figure 3**) [46, 51]. This structure provokes their biaxial character that compromises their crystallization, resulting in internal crack formation when LFZ processing is carried out in air and the cooling is not gradually performed [18, 47]. **Figure 4** shows the XRD powder diffractogram of the Gd, Lu and Nd oxyorthosilicates presented in this chapter. It should be noted

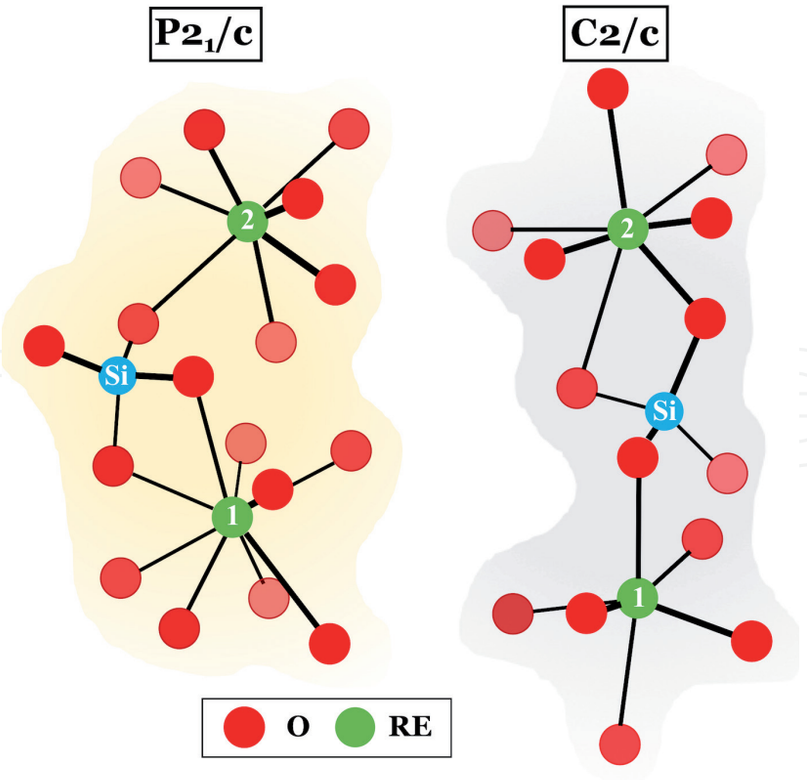

Figure 3.
Structural scheme of P2₁/c and C2/c spatial groups [46].

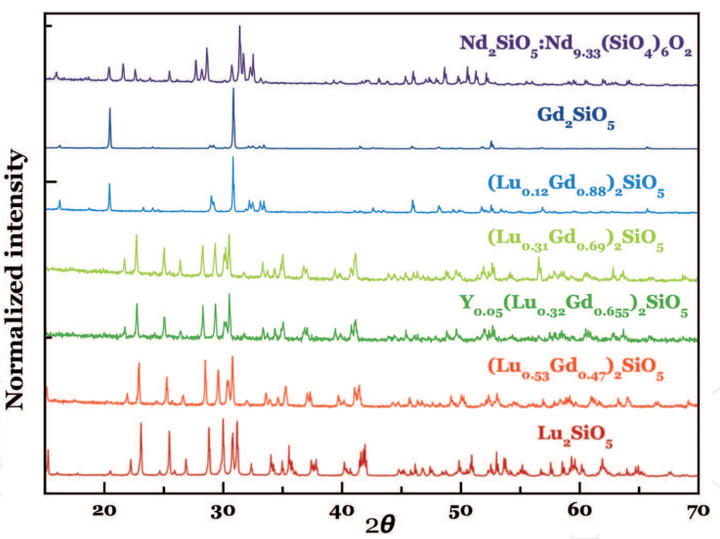

Figure 4.
XRD diffractograms of the oxyorthosilicates produced by LFZ in air at 10 mm h^{-1} [18, 45–47].

that the change from $P2_1/c$ (Gd_2SiO_5 and $(Lu_{0.12}Gd_{0.88})_2SiO_5$) to C2/c space group is most visible in the diffractograms at 2θ ranging from 20 to 30°.

Following the structural overview about oxyorthosilicates, the Raman spectroscopy analysis can be divided in two groups or families considering the total number of vibrational modes together with the shape of the high frequency region. Thus, assuming the Voron'ko et al. [8] notation, oxyorthosilicates can be distinguished among **A-type** and **B-type** silicates depending on whether a triplet or a doublet, respectively, appears inside the ($\nu_1 + \nu_3$) region [8, 9, 18, 45–47]. This way, the Raman spectra can be divided in four vibrational regions denoted as ν_3, ($\nu_1 + \nu_3$), ν_4 and $\nu_{ext} + \nu_2$ (**Figure 5**) [8]. The modes (ν_1)–(ν_4) correspond to free internal vibrations of the

tetrahedral $[SiO_4]^{4-}$ complex in the reduced C_1 symmetry of the monoclinic lattice, while the external oscillations produced by the translation of the $[MO_4]$-complexes are ascribed to the ν_{ext} mode [8, 46, 52]. In addition, the modes related to rare earth ions and RE-O stretching vibrations are also placed inside the (ν_{ext} + ν_2) region.

4.1 Gadolinium oxyorthosilicate (GSO)

One of the most important oxyorthosilicates is gadolinium silicate (Gd_2SiO_5, GSO) due to the Gd^{3+} charger transfer band (CTB) that favors the transfer processes from the ground state $^8S_{7/2}$ to energy levels of the dopant element [48–50]. Transparent crystalline fibers with a yellowish aspect at naked eye (**Figure 6a**) were grown in 2017 by Rey-García et al. [18] using the LFZ technique. These fibers present a similar aspect to the ones obtained by Takagi et al. using Czochralski method [53]. Moreover, the LFZ fibers were developed in air at higher pulling rates. SEM analysis reveals a homogeneous fiber without visible grain boundaries (**Figure 6b**), thus suggesting a single crystal character. Furthermore, the EDS analysis performed confirms this homogeneity and putting in evidence the uniform elemental composition corresponding to Gd_2SiO_5 stoichiometry.

Following the structural analysis, the XRD powders diffractogram shown in **Figure 3** well matches with the 04–009-2670 XRD card (International Centre for Diffraction Data, 2019 [54]) putting in evidence the crystallinity and the monophasic nature of the monoclinic $P2_1/c$ $Gd_2(SiO_4)O$ oxyorthosilicate. Moreover, XRD scan along the longitudinal section of a polished fiber matching the diffraction maxima corresponding to {h 0 0} planes, suggesting a monocrystalline character. Aiming to confirm this evidence, 3D pole figures on longitudinal and transversal cross sections of the fibers were acquired (**Figure 7**). The crystallographic texture measurements confirmed the production of Gd_2SiO_5 single crystal fibers by LFZ, since only one high intense peak was observed in both sections. This type of morphology is potentiated by the strong thermal gradient that exists at the crystallization interface in the LFZ process [55]. So, in conclusion, these observations, namely the preferential orientation and the absence of grain boundaries in SEM analysis, permit to confirm the single crystal character of the GSO fibers grown by LFZ. In addition, the Raman spectroscopy analysis (**Figure 5**) of the GSO samples put in evidence several narrow lines, as expected for a low-symmetry crystalline structure [18].

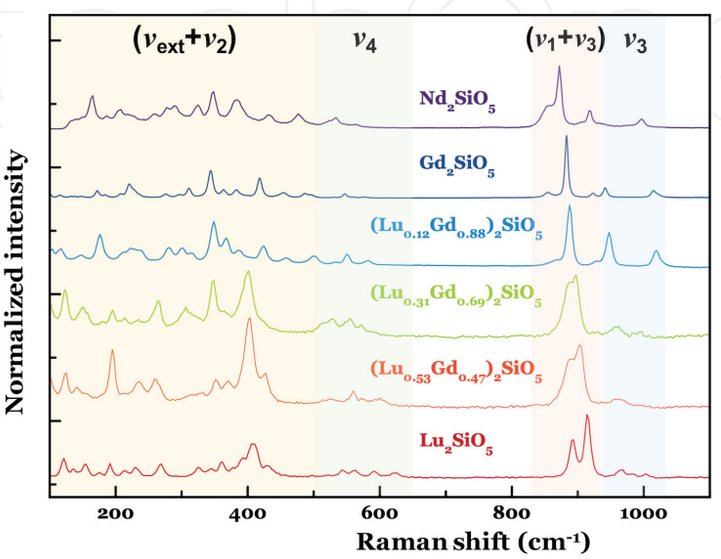

Figure 5.
Raman spectra performed under excitation of 441.6 nm line of a He-Cd laser (Kimmon IK series) of the oxyorthosilicates grown in air by LFZ [18, 45–47].

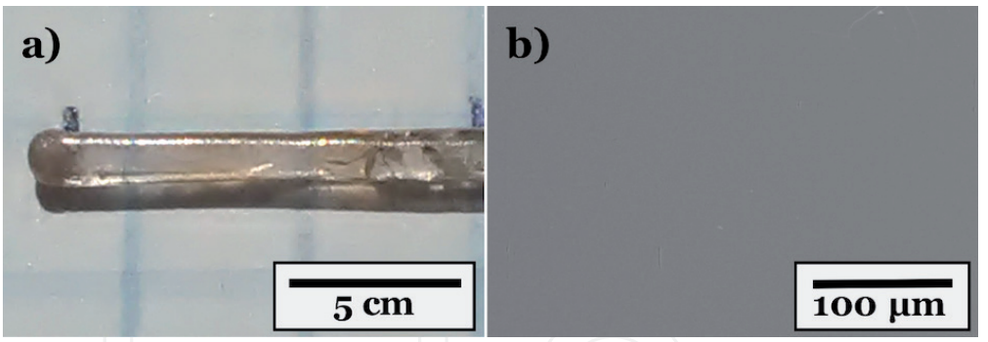

Figure 6.
(a) Photograph of GSO sample [18] and (b) corresponding SEM micrograph.

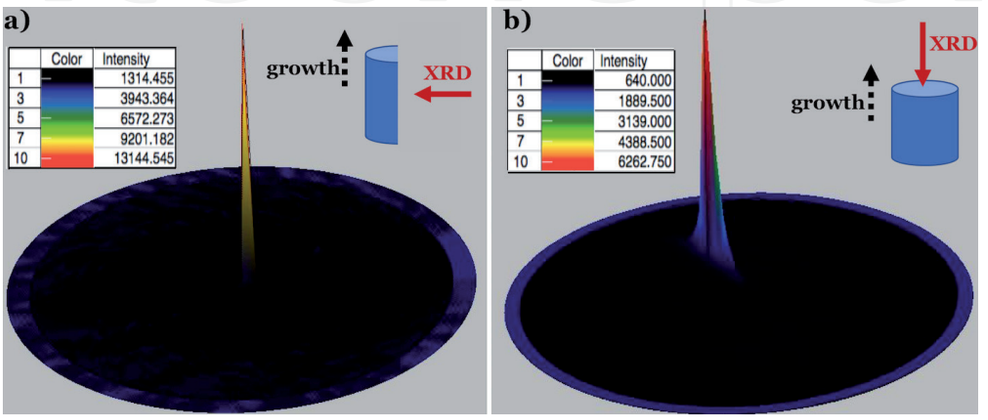

Figure 7.
XRD 3D pole figures of (a) longitudinal section, obtained for 2θ = 30.7°, corresponding to the (3 0 0) plane and (b) transversal cross section for (1 2 1) crystallographic plane of GSO fiber [18].

The optical spectroscopy characterization, performed from the ultraviolet to the near infrared spectral region, by photoluminescence and photoluminescence excitation suggests that GSO fibers are in fact suitable materials to be doped with rare earth active ions envisaging developing optical efficient laser materials [18]. The spectrum is mainly characterized by a series of sharp lines in the ultraviolet region corresponding to the intra $4f^7$ transitions of the Gd^{3+} ions. In fact, their excitation with ultraviolet photons promotes intra $4f^7$ transitions of the Gd^{3+} ions, and therefore, the energy transfer observed provokes internal f→f transitions of trivalent dopant ions [56–58].

4.2 Lutetium and gadolinium oxyorthosilicate (LGSO)

The interest of researchers has progressively gone *in crescendo* to mixed oxyorthosilicates of lutetium and gadolinium (LGSO) [1, 9, 59, 60] due to the following reasons:

i. Lu_2O_3 precursor is expensive, increasing the production cost of photonic materials. This way, the co-doping with gadolinium ions, using as raw material Gd_2O_3, allows reducing the cost without affecting the structural and optical properties.

ii. Gadolinium oxyorthosilicate single crystals tend to develop cracks during growth. Considering this handicap, lutetium doping has been employed aiming to reduce thermal stress and, therefore, avoiding crack formation.

iii. Finally, comparing the melting points of Lu_2O_3 (2490°C) and Gd_2O_3 (2420°C), the introduction of the second one on pure LSO materials should slightly reduce the LGSO melting point.

Analogous to what has been previously mentioned, Czochralski (CZ) method has been extensively used to develop LGSO [1, 9, 52] since Loutts et al. [61] produced LGSO for the first time in 1997. Thus, lutetium-gadolinium oxyorthosilicate crystalline fibers were successfully produced by LFZ in air at 10 mm h^{-1} [46]. Thus, three compositions based on $(Lu_xGd_{1-x})_2SiO_5$ formula were developed, establishing the doping level as x = 0.1 (LGSO-1), 0.3 (LGSO-3) and 0.5 (LGSO-5). Plane parallel-polished fragments of each one is shown in **Figure 8**. The transparency degree is clearly observed at naked eye, being not gradual with lutetium amount. In fact, LGSO-1 and LGSO-5 are translucent fibers, owning the first a yellowish tone like to that observed for pure GSO fibers. On the other hand, LGSO-3 sample is transparent, being distinguishable the colors and letters of the background image. Transmission spectra (**Figure 8**) corroborate this appearance. Transmittance values from 50% up to 77% along the visible range are observed. In addition, it must be noted that the transfer bands of the Gd^{3+} have resulted for the LGSO-3 fibers higher in intensity than pure GSO, highlighting this crystal as optimal host laser material.

On the other hand, the EDS analysis shown that LGSO crystalline fibers produced by LFZ present compositions close to the initial mixtures, in opposite to compositional dissimilarity observed on LGSO materials developed by conventional CZ method [1, 9, 52]. The expected structural change at x = 0.17 coming from the Lu amount matches with that reported by literature [1, 9, 52, 62]. Thus, LGSO-1 presents the monoclinic $P2_1/c$ structure, while the other two have a monoclinic C2/c structure, as can be deduced from the diffractograms shown in **Figure 4**. This way, LGSO-1 matched with the 01-080-9851 XRD card ICDD, while LGSO-3 and LGSO-5 are isostructural with the 00-061-0488 and the 00-061-0369 XRD cards, respectively [54].

The phase transition observed with lutetium addition is explained from atomic size and the differences of nearest surrounding rare earth ions, as reported Ryba-Romanowski et al. [63]. In fact, GSO lattice present Gd1 and Gd2 sites with different coordination number and local symmetries (CN = 9, C_{3v} and CN = 7, C_s, respectively), promoting the polyhedrons GdO_9 and GdO_7. On the other side, LSO

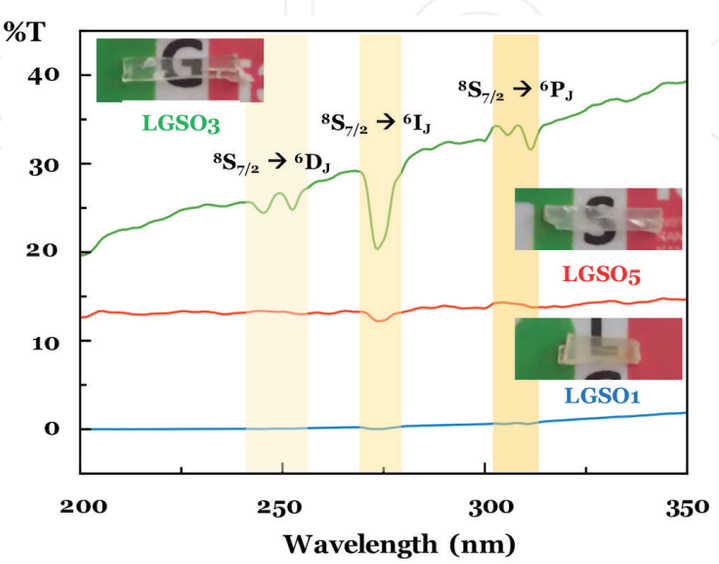

Figure 8.
Transmission spectra and photographs of LGSO fibers in the UV range [46].

lattice present both lutetium ions, and therefore, the LuO_6 (Lu1) and LuO_7 (Lu2) polyhedrons present the C_s local symmetry. The former has only one plane of symmetry, while the C_{3v} point group presents higher steric effect. Additionally, despite the smaller ionic radius of the Lu^{3+}, its inclusion into the monoclinic $P2_1/c$ unit cell strongly affects the crystalline structure. Concomitantly, the GSO structure type allows low Lu doping. In opposite, the C2/c type structure presents minor steric effect and higher symmetry degrees of freedom, allowing the introduction of large size ions such as Gd^{3+} or Ce^{3+} on the Lu sites. Consequently, LGSO-3 and LGSO-5 samples have the C2/c crystalline structure, which is larger in size than $P2_1/c$ (**Table 2**). On the other hand, **Table 2** shows how introduction of Lu decreases the volume of the cell together with an increase of the density. Concerning Raman spectroscopy characterization, LGSO-3 sample presents an intermediate spectrum between the GSO and LSO (**Figure 5**). In fact, when ($\nu_1 + \nu_3$) region is revised, LGSO-1 relates to A-type, like GSO structure, while LGSO-3 and LGSO-5 spectrum shape shows the typical doublet of B-type silicates, such as undoped LSO. Finally, the transmission studies of LGSO samples allow concluding that the Gd^{3+} ions are optically active. In fact, an intra-ionic absorption due to the energy transfer band ascribed to $^8S_{7/2} \rightarrow {}^6I_J$ transition is observed, and this band is the highest for LGSO-3 sample, the one that is the most transparent and presents lower cracks. All these considerations allow to consider the LGSO-3 fibers as the most suitable host material for photonic applications [46].

4.3 Rare-earth-doped lutetium and gadolinium oxyorthosilicates (LGSO:RE)

Once the best laser host properties were determined by developing the initial Gd_2SiO_5 to the $(Lu_{0.3}Gd_{0.7})_2SiO_5$ compositions, together with the enhancement of the structural and morphological characteristics, the scientific interest was centered in a designed doping strategy considering the most suitable rare earth ions (RE = Nd, Y and Yb).

4.3.1 Yttrium-doped (LGSO:Y)

Yttrium was selected as a dopant, since it promotes an excellent thermal and optical properties [47], being usually introduced in oxide form as a stabilizing agent. In fact, it has been largely employed in laser materials, namely yttrium aluminum garnets (YAG) or thermal barrier coatings (TBCs) due to its good thermal conductivity (13.6 W m^{-1} K^{-1}), shock resistance and low thermal expansion coefficient [64–66]. Additionally, its melting point (2425°C) is close to the one of Gd_2O_3 (2430°C).

Crystal	R_{exp} (%)	R_p (%)	R_{wp} (%)	GOF	a (Å)	b (Å)	c (Å)	Volume (10^6 pm^3)	Density (g cm^{-3})
GSO	2.82	4.23	5.70	2.08	9.128	7.058	6.746	414.26	6.775
LGSO1	2.56	2.68	3.39	1.26	9.123	7.021	6.738	411.69	6.954
LGSO3	3.33	3.75	5.29	1.59	14.461	6.750	10.495	867.06	6.570
LGSOY	2.22	3.05	4.07	1.83	14.457	6.749	10.491	866.32	6.576
LGSO5	3.29	4.23	5.51	1.68	14.391	6.716	10.425	852.72	6.949

The conventional agreement indices R_{exp}, R_p and R_{wp} correspond to the expected, profile and weighted profile R-factors, respectively. The GOF parameter represents the goodness of fit.

Table 2.
Refined unit cell parameters and relative densities of GSO and lutetium and yttrium-doped single crystals calculated from XRD analysis in powders [18, 46, 47].

The introduction of yttrium should bring stress hampering, maintaining the role of a laser passive element, by substitution of Lu^{3+} ions due to their similar atomic radius (212 pm for Y^{3+} and 217 pm for Lu^{3+}) and considering that Y_2SiO_5 has C2/c monoclinic structure. Thus, the introduction of 5 mol% of yttrium provoked a significant increase on transparency, with transmittance values around 86% along the visible range, and also reducing or even avoiding crack formation when compared with the pure LGSO (**Figure 8**). As additional advantage, the relative absorption intensity of the charge transfer bands of the Gd^{3+} ions, namely the intra $4f^7$ transitions, has been significantly increased (**Figure 9**), enhancing their suitability as matrix [47].

On the other side, the introduction of yttrium does not bring significant modifications in the lattice structure of the crystal, since XRD powder diffractogram of the LGSO:Y totally matches with the 00-061-0488 ICDD XRD card like the LGSO-3 single crystal fiber [54], and the Rietveld refinement shows similar unit cell parameters for both materials (**Table 2**). Indeed, Y^{3+} ions have substituted Gd^{3+} ions due to their close ionic radii (0.90 Å and 0.94 Å in a 6-fold coordination, respectively) along with similar electronegativity values (1.22 and 1.20, respectively) [67]. Concomitantly, Y^{3+} has increased plasticity, thus reducing stress, minimizing crack formation and maintaining the C2/c monoclinic structure.

4.3.2 Neodyminum (LGSO:Nd) and ytterbium-doped (LGSO:Yb)

It should be noted that the approach presented here is in production process.

Following the doping strategy for the $(Lu_{0.3}Gd_{0.7})_2SiO_5$ (LGSO-3) matrix, the next step was the doping with laser active elements such as Nd^{3+} and Yb^{3+} aiming to produce laser active materials. These dopants are extensively used as emitting ions in several laser materials [4–6, 33, 34] produced by different crystallization methods. Indeed, de la Fuente et al. [33] and Black et al. [34] produced $GdNdSiO_5$ and $7Gd_2O_3•9SiO_2$:Nd single crystal laser materials by LFZ in $Ar:O_2$ atmospheres 30 years ago. However, most researchers employed standard growth methods. For example, Xu et al. [5] produced a controllable dual-wavelength continuous-wave laser emitting at 1075 and 1079 nm achieving an optical-to-optical efficiency of 63.3% for a $Nd:Lu_2SiO_5$ crystal grown by CZ, in which a peak power of 2.34 kW was measured under passively Q-switched operation. On the other side, Kim

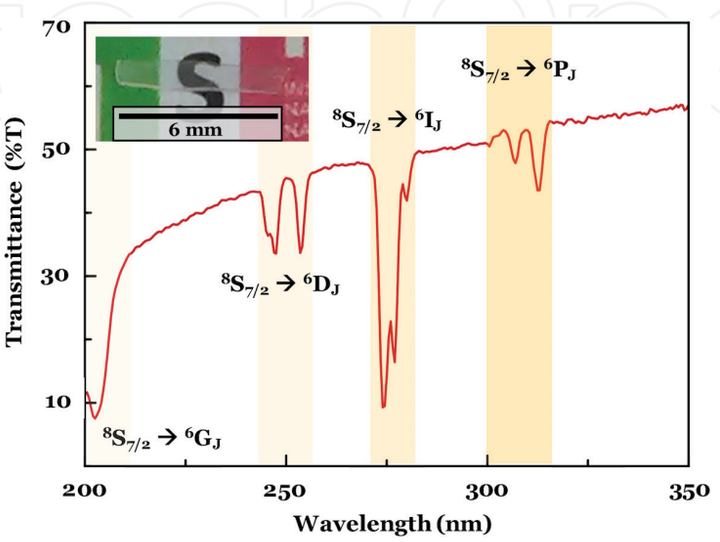

Figure 9.
Crystal photograph and transmission spectrum of LGSO:Y [47].

et al. [6] produced by hot-pressing a 10% Yb:Lu_2O_3 laser crystal pumped at 975 nm and emitting at 1080 nm presenting a slope efficiency of 74% with an output power of 16 W.

Considering the previous results of LGSO-3 samples, new powder mixtures were prepared by doping with 5 mol% of Nd_2O_3 and Yb_2O_3, using highly pure (5 N) oxide powders. Thus, neodymium (LGSO:Nd) and ytterbium (LGSO:Yb) doped LGSO single crystal fibers were produced by LFZ in air at 10 mm h^{-1}. However, these crystals present lower optical quality than those of LGSO doped with yttrium. The absorption of the LGSO:Yb crystals checked in a Z-cavity varied between 35 and 50% for a pumping of 978 nm Ti-sapphire laser, emitting at ~1039 nm wavelength (**Figure 10a**). On the other hand, LGSO:Nd diode pumped at 811 nm emits at ~1076 nm wavelength and absorbs 80% (**Figure 10b**).

4.4 Lutetium oxyorthosilicate (LSO)

Lutetium oxyorthosilicate (Lu_2SiO_5, LSO) has attracted the attention of researchers due to their favorable thermal and optical properties, which make it suitable as host materials to be used in photonics as laser media [3–6] or scintillators [7, 41, 59]. The main technique for producing LSO crystals is usually the CZ method. As an alternative, Farhi et al. [68] in 2008 grew by laser-heated pedestal growth (LHPG) rods of LSO and LSO:Ce^{3+} in air and N_2 atmosphere at 15 mm h^{-1} from square feed rods cut from a LSO pellet prepared by solid state reaction. Thus, it was expected that these type of oxyorthosilicates could be produced in air at 10 mm h^{-1} like the GSO. However, despite the fibers grown at 200 and 100 mm h^{-1} by the LFZ technique present a translucent aspect, the fibers obtained at lower pulling rates (10 and 5 mm h^{-1}) are white and opaque (insets of **Figure 11**) [45]. SEM and EDS analysis of the samples produced by LFZ put in evidence a transition from single crystal to eutectic ceramics with the gradual appearance of the Lu_2O_3 phase into the Lu_2SiO_5 matrix as pulling rate is decreased. The eutectics present a banded structure of alternated monophasic oxyorthosilicate regions with a biphasic Lu_2SiO_5/Lu_2O_3 phases. The presence of both phases was also corroborated by XRD analysis [45].

The strong difference between the melting points of both precursors, SiO_2 (1710°C) and Lu_2O_3 (2490°C), explains this behavior. In fact, the high laser power necessary to melt lutetium oxide induces SiO_2 evaporation, by overheating during laser processing. This phenomenon was already observed by Farhi et al. [68]. The most volatile compounds tend to evaporate due to overheating when two materials

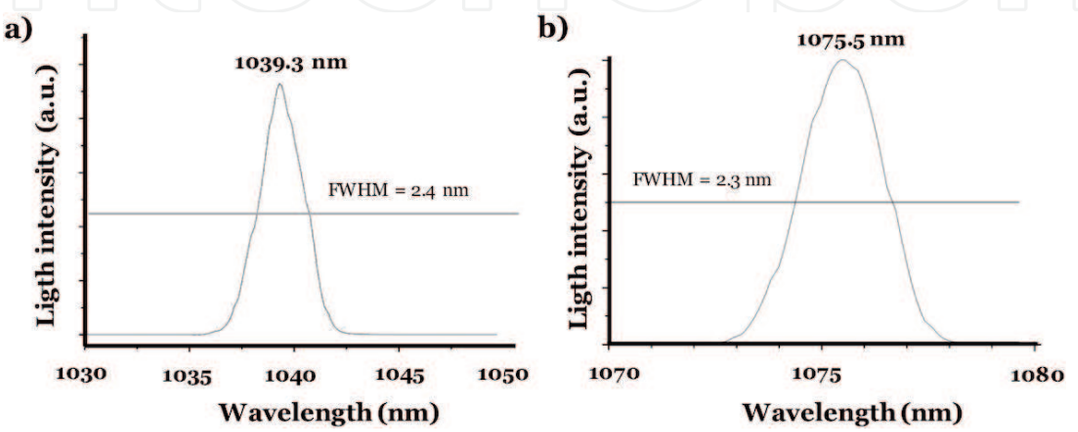

Figure 10.
Emitting wavelength of (a) LGSO:Yb and (b) LGSO:Nd crystals.

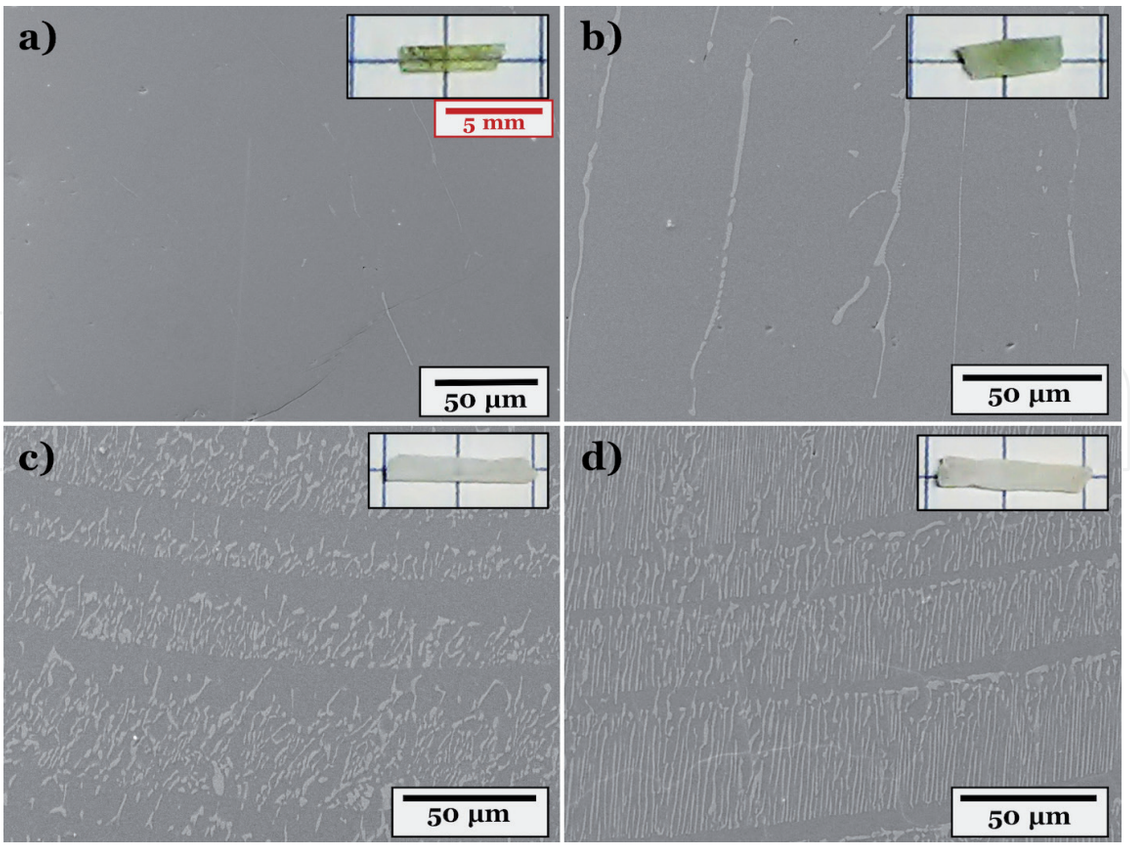

Figure 11.
SEM micrographs and photographs of LSO samples grown by LFZ at (a) 200 mm h^{-1}, (b) 100 mm h^{-1}, (c) 10 mm h^{-1} and (d) 5 mm h^{-1} [45].

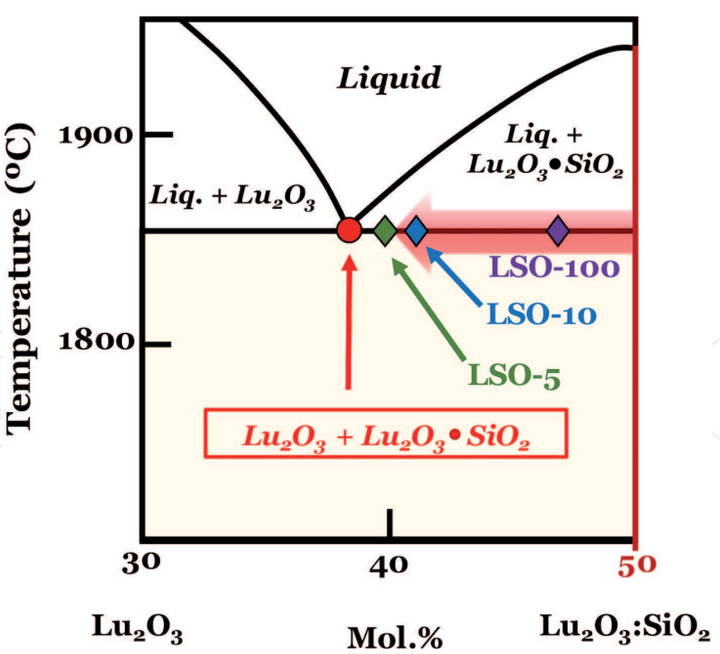

Figure 12.
Compositional deviation from the nominal 1:1 composition to eutectic point (red dot) into the Lu_2O_3-SiO_2 phase diagram based on Yb_2O_3-SiO_2 system [45, 69].

with a great melting point mismatch are processed by LFZ. Concomitantly, a deviation from the nominal composition is observed, and consequently, the as-grown material exhibits a different composition. This is what happened in the Lu_2O_3-SiO_2 system. Consequently, the crystallization path may vary, and therefore, the nature

and amount of solidified phases present in the crystallized material can be different. **Figure 12** puts in evidence the compositional deviation from the nominal composition (Lu_2O_3:SiO_2 = 1:1) toward the eutectic point in the Lu_2O_3-SiO_2 binary phase diagram (red dot). This compositional shift corroborates the SEM images of **Figure 11**, where an almost complete eutectic morphology is achieved in the slower processed fibers, the ones submitted to higher power for longer times. It is noteworthy the preferential alignment of the eutectic constituent, triggered by the strong axial thermal gradients at the solidification interface [70, 71]. The introduction of other rare earth ions such as Nd, with an intermediate melting point (2233°C), contributes to the decrease of the evaporation process, since both Lu_2O_3 lamellae presence inside the Lu_2SiO_5 and their size are reduced in diameter and significantly decreased in number.

Another interesting characteristic of the LSO fibers grown by the LFZ process is a pronounced photochromic effect, from white to pink-reddish tone. This behavior was observed in samples grown at lower pulling rates when irradiated with UV light. This effect persists for samples stored in the dark, even in the presence of oxidant atmosphere, while the bleaching of the photochromic coloration is reversible when samples are under natural illumination (**Figure 13**) [45].

4.5 Neodymium oxyorthosilicate (NSO)

The Nd_2SiO_5 compound has been obtained only by solid state methods and, in the most cases, accompanied by other silicate phases, namely the pyrosilicate $Nd_2Si_2O_7$ [72–74]. In fact, it must be noted that the production of this kind of orthosilicates is hard since the Nd_2O_3-SiO_2 system melts incongruently [73]. Concomitantly, Jiang et al. [74] have recently sintered for microwave device applications, pure Nd_2SiO_5 starting from Nd_2O_3:SiO_2 = 1:1.05 mixtures. A minimum deviation from this ratio promotes the formation of by-products such as $Nd_4Si_3O_{12}$ or Nd_2O_3.

The processing of stoichiometric mixtures of SiO_2 and Nd_2O_3 oxides through the LFZ technique produced large violet fibers. The apparent crystalline aspect of these fibers increases with pulling rate from umber-like (5 and 10 mm h^{-1}) to brighter materials (100–400 mm h^{-1}) (**Figure 14a**). The XRD analysis identified the presence of two phases, which were confirmed by SEM analysis as elongated Nd_2SiO_5 crystals inside of the $Nd_{9.33}(SiO_4)_6O_2$ matrix (**Figure 14b**). The phases present a preferential orientation along the fiber axis. Furthermore, the amount of each phase significantly depends on the pulling rate. Lower pulling rates tend to increase the nonstoichiometric phase, $Nd_{9.33}(SiO_4)_6O_2$.

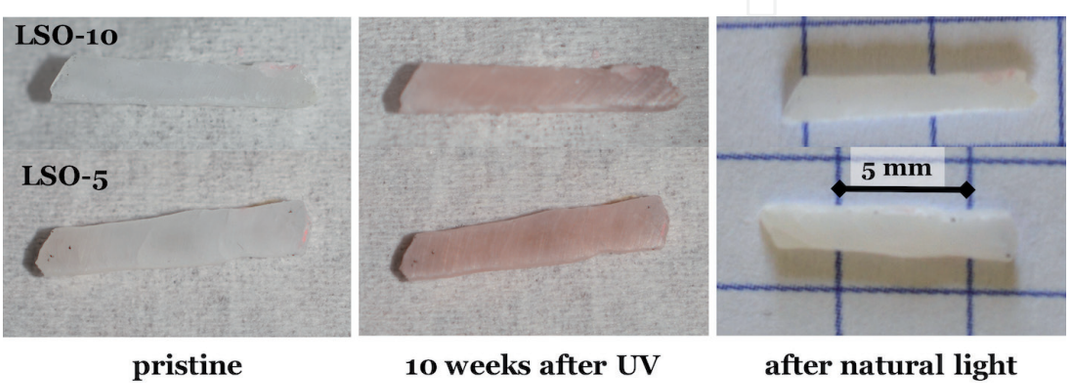

Figure 13.
Photographs of parallel-polished LSO fibers showing photochromic effect after irradiation with UV light (254 nm) [45].

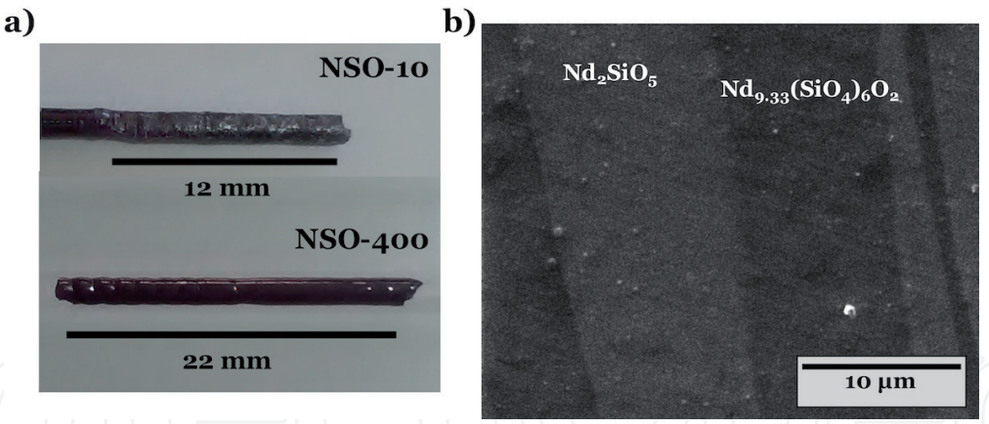

Figure 14.
(a) Photographs of NSO samples grown at 10 (NSO-10) and 400 mm h^{-1} (NSO-400), and (b) SEM micrograph identifying phases present in the NSO fiber.

Envisaging the applications of NSO fiber and considering the opposite electrical behavior of both phases together with the fibers texturing, mainly the ones grown at the highest pulling rate (200 and 400 mm h^{-1}), it is important to study their electrical properties. This way, the electrical conductivity and the dielectric constant were measured from room temperature until 1000°C and varying the frequency from 10^2 to 10^6 Hz. An increase of the AC conductivity with frequency and temperature was observed for all samples. Specifically, at 1000°C and 10 Hz, the electrical conductivity of 10^{-5} S cm^{-1} at room temperature increases to 10^{-2} S cm^{-1}. The NSO fibers exhibit a typical response of ionic conductors [30, 71] with a p-type electronic behavior, according to León-Reina et al. [75] for Nd_2SiO_5 samples. On the other side, the dielectric constant decreases with frequency while an increase with temperature is observed. Values of 10 at room temperature increase up to 10^9 at 1000°C. The high densification degree of fibers and the different polarization mechanisms, as reported Jiang et al. [74], underlie this behavior. This consideration agrees with the typical characteristics of LFZ method that is known to produce samples with a higher density when compared with standard solid state sintering [76]. Additionally, these results confirm local variations in the Nd phases leading to interstitial oxygen variations affecting the electrical response [75, 77].

5. Conclusions

This chapter puts in evidence several advantages of the LFZ technique with respect to standard growth methods. In fact, LFZ is a suitable crystallization technique that allows obtaining highly oriented refractory materials such as the rare earth oxyorthosilicates. Focusing on the special characteristics of the LFZ process and extrapolating to other hard-synthesis materials, the LFZ revealed to be a suitable method for prototyping. This consideration is based on the capabilities that directly promote a reduction of the effective production costs, namely: it is a crucible-free technique, avoiding external contamination; it allows working with low precursors amount, together with the possibility to produce low volume of high-quality materials; it is a fast processing technique that allows reducing processing time; it allows the production of small-in-size high-quality single crystal or highly textured ceramics with an appropriate geometry, allowing the development of compact and miniaturized photonic devices; it allows the growth of directionally solidified eutectic ceramic materials; it allows the crystallization of metastable phases. Thus, it was demonstrated the ability to produce high-quality single crystals

of the $(Lu_{0.3}Gd_{0.7})_2SiO_5$ based composition in air at fast pulling rates. These crystals are suitable as laser passive and gain media. On the other side, Lu_2O_3/Lu_2SiO_5 eutectic ceramics exhibit an interesting reversible photochromic effect. Last, biphasic ceramics of $Nd_2SiO_5/Nd_{9.33}(SiO_4)_6O_2$ suitable for microwave devices can also be synthesized by the LFZ method.

Acknowledgements

F. Rey-García acknowledges the Portuguese Science and Technology Foundation (FCT) for the SFRH/BPD/108581/2015 grant and is grateful to funding from EU (project SPRINT, EU H2020-FET-OPEN/0426). C. Bao-Varela acknowledges funds from Xunta de Galicia (ED431E 2018/08) and Consellería de Cultura, Educación e Ordenación Universitaria (ED431B 2017/64). F.M. Costa acknowledges financial support from FEDER funds through the COMPETE 2020 Programme and National Funds through FCT—Portuguese Foundation for Science and Technology under the projects UID/CTM/50025/2019 and POCI-01-0145-FEDER-028755.

Author details

Francisco Rey-García[1*], Carmen Bao-Varela[2] and Florinda M. Costa[3]

1 Instituto de Ciencia de Materiales de Aragón (ICMA-CSIC), Zaragoza, Spain

2 UA Microoptics and GRIN Optics group (ICMA-CSIC), Universidade de Santiago de Compostela, Santiago de Compostela, Spain

3 i3N and Physics Department, Universidade de Aveiro, Aveiro, Portugal

*Address all correspondence to: francisco.rey.usc@gmail.com

References

[1] Ryba-Romanowski SA, Lisiecki R, Berkowski M, Rodriguez-Rodriguez H, Martin IR. Effect of substitution of lutetium by gadolinium on emission characteristics of $(Lu_xGd_{1-x})_2SiO_5:Sm^{3+}$ single crystals. Optical Materials Express. 2014;**4**:739-752. DOI: 10.1364/OME.4.000739

[2] Kobayashi K, Sakka Y. Research progress in nondoped lanthanoid silicate oxyapatites as new oxygen-ion conductors. Journal of the Ceramic Society of Japan. 2004;**122**:921-939. DOI: 10.2109/jcersj2.122.921

[3] Zheng L, Su L, Growth XJ. Characterization of ytterbium doped silicate crystals for ultra-fast laser applications. In: Kolesnikov N, Borisenko E, editors. Modern Aspects of Bulk Crystal and Thin Film Preparation. Rijeka: IntechOpen; 2012. pp. 25-42. DOI: 10.5772/30457

[4] Li DZ, Xu XD, Zhou DH, Xia CT, Wu F, Xu J, et al. Crystal growth, optical properties, and continuous-wave laser operation of Nd^{3+}-doped Lu_2SiO_5 crystal. Laser Physics Letters. 2011;**8**: 32-37. DOI: 10.1002/lapl.201010092

[5] Xu X, Di J, Zhang J, Tang D, Xu J. CW and passively Q-switched laser performance of Nd:Lu_2SiO_5 crystal. Optical Materials. 2016;**51**:241-244. DOI: 10.1016/j.optmat.2015.11.008

[6] Kim W, Villalobos G, Baker C, Frantz J, Shaw B, Bayya S, et al. Overview of transparent optical ceramics for high-energy lasers at NRL. Applied Optics. 2015;**54**:F210-F221. DOI: 10.1364/AO.54.00F210

[7] Jary V, Krasnikov A, Nikl M, Zazubovich S. Origin of slow low-temperature luminescence in undoped and Ce-doped Y_2SiO_5 and Lu_2SiO_5 single crystals. Physica Status Solidi B: Basic Solid State Physics. 2015;**252**:274-281. DOI: 10.1002/pssb.201451234

[8] Voron'ko YK, Sobol AA, Shukshin VE, Zagumennyi AI, Zavartsev YD, Koutovoi SA. Spontaneous Raman spectra of the crystalline, molten and vitreous rare-earth oxyorthosilicates. Optical Materials. 2011;**33**:1331-1337. DOI: 10.1016/j.optmat.2011.03.021

[9] Bińczyk M, Glowacki M, Lapiński A, Berkowski M, Runka T. μ-Raman and infrared reflectance spectroscopy characterization of $(Lu_{1-x}Gd_x)_2SiO_5$ solid solution single crystals doped with Dy^{3+} or Sm^{3+}. Journal of Molecular Structure. 2016;**1109**:50-57. DOI: 10.1016/j.molstruc.2015.12.078

[10] Kamada K, Murakami R, Kochurikhin VV, Luidmila G, Kim KJ, Shoji Y, et al. Single crystal growth of submillimeter diameter sapphire tube by the micro-pulling down method. Journal of Crystal Growth. 2018;**492**:45-49. DOI: 10.1016/j.jcrysgro.2018.03.023

[11] Masubuchi Y, Higuchi M, Katase H, Takeda T, Kikkawa S, Kodaira K, et al. Oxide ion conduction in $Nd_{9.33}(SiO_4)_6O_2$ and $Sr_2Nd_8(SiO_4)_6O_2$ single crystals grown by floating zone method. Solid State Ionics. 2004;**166**:213-217. DOI: 10.1016/j.ssi.2003.09.019

[12] Liu QY, Liu ZY, Zhou XB, Liu ZG, Huo MX, Wang XJ, et al. Large size single crystal growth of Ti_4O_7 by the floating-zone method. Crystal Growth & Design. 2019;**19**:730-736. DOI: 10.1021/acs.cgd.8b01318

[13] Carvalho RG, Pires MS, Fernandes AJS, Silva RF, Costa FM. Directionally solidified eutectic and off-eutectic mullite-zirconia fibres. Journal of the European Ceramic Society. 2013;**33**:953-963. DOI: 10.1016/j.jeurceramsoc.2012.09.032

[14] Andreeta MRB, Hernandes AC. Laser-heated pedestal Growth of oxide Fibers. In: Dhanaraj G, Byrappa K, Prasad V, Dudley M, editors. Springer Handbook of Crystal Growth. Berlin: Springer; 2010. pp. 393-432. DOI: 10.1007/978-3-540-74761-1_13

[15] Soares MRN, Soares MJ, Fernandes AJS, Rino L, Costa FM, Monteiro T. YSZ: Dy^{3+} single crystal white emitter. Journal of Materials Chemistry. 2011;**21**:15262-15265. DOI: 10.1039/C1JM12564H

[16] Carvalho RG, Fernandes AJS, Oliveira FJ, Alves E, Franco N, Louro C, et al. Single and polycrystalline mullite fibres grown by laser floating zone technique. Journal of the European Ceramic Society. 2010;**30**:3311-3318. DOI: 10.1016/j.jeurceramsoc.2010.07.033

[17] Soares MRN, Nico C, Peres M, Ferreira N, Fernandes AJS, Monteiro T, et al. Structural and optical properties of europium doped zirconia single crystals fibers grown by laser floating zone technique. Journal of Applied Physics. 2011;**109**:013516. DOI: 10.1063/1.3527914

[18] Rey-García F, Ben Sedrine N, Soares MR, Fernandes AJS, Lopes AB, Ferreira NM, et al. Structural and optical characterization of Gd_2SiO_5 crystalline fibres obtained by laser floating zone. Optical Materials Express. 2017;**7**:868-879. DOI: 10.1364/OME.7.000868

[19] Costa FM, Silva RF, Vieira JM. Diffusion phenomena and crystallization path during the growth of LFZ Bi-Sr-Ca-Cu-O superconducting fibres. Superconductor Science and Technology. 2001;**14**:910-920. DOI: 10.1088/0953-2048/14/11/305

[20] Edmonds WR. The reflaxicon, a new reflective optical element and some applications. Applied Optics. 1973;**12**:1940-1944. DOI: 10.1364/AO.12.001940

[21] Martin CW. Reflecting Optical Objective System. U.S. Patent 2457253. 1948.

[22] Ferreira NM, Kovalevsky AV, Costa FM, Frade JR. Processing effects on properties of $(Fe,Mg,Al)_3O_4$ spinels as potential consumable anodes for pyroelectrolysis. Journal of the American Ceramic Society. 2016;**99**:1-5. DOI: 10.1111/jace.14190

[23] Carrasco MF, Silva RF, Vieira JM, Costa FM. Electrical field freezing effect on laser floating zone (LFZ)-grown $Bi_2Sr_2Ca_2Cu_4O_{11}$ superconducting fibres. Superconductor Science and Technology. 2004;**17**:612-619. DOI: 10.1088/0953-2048/17/4/008

[24] Carrasco MF, Silva RF, Vieira JM, Costa FM. Pulling rate and current intensity competition in electrically assisted laser floating zone. Superconductor Science and Technology. 2009;**22**:065016. DOI: 10.1088/0953-2048/22/6/065016

[25] Ferreira NM, Rasekh S, Costa FM, Madre MA, Sotelo A, Diez JC, et al. New method to improve the grain alignment and performance of thermoelectric ceramics. Materials Letters. 2012;**83**:144-147. DOI: 10.1016/j.matlet.2012.05.131

[26] Costa FM, Ferreira NM, Rasekh S, Fernandes AJS, Torres MA, Madre MA, et al. Very large superconducting currents induced by growth tailoring. Crystal Growth & Design. 2015;**15**:2094-2101. DOI: 10.1021/cg5015972

[27] Graça MPF, Peixoto MV, Ferreira N, Rodrigues J, Nico C, Costa FM, et al. Optical and dielectric behaviour of $EuNbO_4$ crystals. Journal of Materials Chemistry C. 2013;**1**:2913-2919. DOI: 10.1039/C3TC00793F

[28] Soares MRN, Nico C, Rodrigues J, Peres M, Soares MJ, Fernandes AJS, et al. Bright room-temperature green luminescence from YSZ:Tb^{3+}. Materials Letters. 2011;**65**:1979-1981. DOI: 10.1016/j.matlet.2011.03.099

[29] Rasekh S, Costa FM, Ferreira NM, Torres MA, Madre MA, Diez JC, et al. Use of laser technology to produce high thermoelectric performances in $Bi_2Sr_2Co_{1.8}O_x$. Materials and Design. 2015;**75**:143-148. DOI: 10.1016/j.matdes.2015.03.005

[30] Carvalho RG, Fernandes AJS, Silva RF, Costa FM, Figueiredo FM. Directional solidification of ZrO_2-$BaZrO_3$ composites with mixed protonic-oxide ionic conductivity. Solid State Ionics. 2014;**262**:654-658. DOI: 10.1016/j.ssi.2013.10.051

[31] Kobayashi K, Sakka Y. Rudimental research progress of rare-earth silicate oxyapatites: Their identification as a new compound until discovery of their oxygen ion conductivity. Journal of the Ceramic Society of Japan. 2014;**122**:649-663. DOI: 10.2109/jcersj2.122.649

[32] Toropov NA, Bondar IA. Lanthanum silicate $2La_2O_3$•$3SiO_3$. Bulletin of the Academy of Sciences of the USSR, Division of Chemical Science. 1959;**8**:528-530

[33] De La Fuente GF, Black LR, Andrauskas DM, Verdún HR. Growth of Nd-doped rare earth silicates by the laser floating zone method. Solid State Ionics. 1989;**32-33**:494-505. DOI: 10.1016/0167-2738(89)90261-0

[34] Black LR, Andrauskas DM, de la Fuente GF, Verdún HR. Laser heated pedestal growth of Nd-doped oxide crystals for diode pumping. In: Proceedings SPIE 1104, Growth, Characterization, and Applications of Laser Host and Nonlinear Crystals. 1989. p. 175. DOI: 10.1117/12.960593

[35] Duan X, Qian C, Shen Y, Su L, Zheng L, Li L, et al. Efficient Ho:$(Sc_{0.5}Y_{0.5})_2SiO_5$ laser at 2.1 μm in-band pumped by Tm fiber laser. Optics Express. 2019;**27**:4522-4527. DOI: 10.1364/OE.27.004522

[36] Seminko V, Maksimchuk P, Bespalova I, Malyukin Y. Different roles of Ce^{3+} optical centers in oxyorthosilicate nanocrystals at X-ray and UV excitation. Crystals. 2019;**9**:114. DOI: 10.3390/cryst9020114

[37] Ren X, Tian Z, Zhang J, Wang J. Equiatomic quaternary $(Y_{1/4}Ho_{1/4}Er_{1/4}Yb_{1/4})_2SiO_5$ silicate: A perspective multifunctional thermal and environmental barrier coating material. Scripta Materialia. 2019;**168**:47-50. DOI: 10.1016/j.scriptamat.2019.04.018

[38] Zhou PQ, Wang XJ, He YD, Wu ZF, Du JL, Fu EG. Effect of deposition mechanisms on the infrared photoluminescence of erbium-ytterbium silicate films under different sputtering methods. Journal of Applied Physics. 2019;**125**:175114. DOI: 10.1063/1.5089677

[39] Hopkins RH, Rowland GW, Steinbruege KB, Partlow WD. Silicate oxyapatites: New high-energy storage laser host for Nd^{3+}. Journal of the Electrochemical Society. 1971;**118**: 637-639. DOI: 10.1149/1.2408128

[40] Wallenberger FT. Commercial and experimental glass fibers. In: Wallenberger FT, Bingham PA, editors. Fiberglass and Glass Technology. Boston, MA: Springer; 2010. pp. 3-90. DOI: 10.1007/978-1-4419-0736-3_1

[41] Wu Y, Koschan M, Foster C, Melcher CL. Czochralski growth, optical, scintillation, and defect properties of Cu^{2+} codoped Lu_2SiO_5:Ce^{3+} single crystals. Crystal Growth & Design.

2019;**19**:4081-4089. DOI: 10.1021/acs.cgd.9b00479

[42] Haile HT, Dejene FB. Effect of substrate temperature on the material properties of the Y_2SiO_5: Ce^{3+} thin film by pulsed laser deposition (PLD) method. Optik. 2019;**184**:508-517. DOI: 10.1016/j.ijleo.2019.05.003

[43] Jiang F, Cheng L, Wei H, Wang Y. Hot corrosion behavior of Lu_2SiO_5 and La_2SiO_5 in a molten Na_2SO_4 environment: A first-principles corrosion resistance investigation. Ceramics International. 2019;**45**:15532-15537. DOI: 10.1016/j.ceramint.2019.05.058

[44] Nieai AA, Mohammadi M, Bahaabad MS, Arefi AH. Synthesis and characterization of spherical Yb_2SiO_5 powder using solid-state diffusional reaction and spray dry process. Journal of the Australian Ceramic Society. 2019:1-8. DOI: 10.1007/s41779-019-00353-3

[45] Rey-García F, Ben Sedrine N, Fernandes AJS, Monteiro T, Costa FM. Shifting Lu_2SiO_5 crystal to eutectic structure by laser floating zone. Journal of the European Ceramic Society. 2018;**38**:2059-2067. DOI: 10.1016/j.jeurceramsoc.2017.11.003

[46] Rey-García F, Fernandes AJS, Costa FM. Influence of Lu content on $(Lu_xGd_{1-x})_2SiO_5$ oxyorthosilicates grown by laser floating zone: Structural studies and transparency. Materials Research Bulletin. 2018;**112**:413-419. DOI: 10.1016/j.materresbull.2018.04.058

[47] Rey-García F, Rodrigues J, Fernandes AJS, Soares MR, Monteiro T, Costa FM. $(Lu_{0.3}Gd_{0.7})_2SiO_5$:$Y^{3+}$ single crystals grown by the laser floating zone method: Structural and optical studies. CrystEngComm. 2018;**20**:7386-7394. DOI: 10.1039/C8CE01319E

[48] Ananias D, Kostova M, Almeida Paz FA, Ferreira A, Carlos LD, Klinowski J, et al. Photoluminescent layered lanthanide silicates. Journal of the American Chemical Society. 2004;**126**:10410-10417. DOI: 10.1021/ja047905n

[49] Sá Ferreira RA, Karmaoui M, Nobre S, Carlos LD, Pinna N. Optical properties of lanthanide-doped lamellar nanohybrids. ChemPhysChem. 2006;**7**:2215-2222. DOI: 10.1002/cphc.200600317

[50] Hernández-Adame L, Méndez-Blas A, Ruiz-García J, Vega-Acosta JR, Medellín-Rodríguez FJ, Palestino G. Synthesis, characterization, and photoluminescence properties of Gd:Tb oxysulfide colloidal particles. Chemical Engineering Journal. 2014;**258**:136-145. DOI: 10.1016/j.cej.2014.07.067

[51] Springer Materials [Internet]. 2019. Available from: https://materials.springer.com [Accessed: 01 August 2019]

[52] Dominiak-Dzik G, Ryba-Romanowski W, Lisiecki R, Solarz P, Macalik B, Berkowski M, et al. The Czochralski growth of $(Lu_{1-x}Gd_x)_2SiO_5$:Dy single crystals: Structural, optical, and dielectric characterization. Crystal Growth & Design. 2010;**10**:3522-3530. DOI: 10.1021/cg100429b

[53] Takagi K, Fukuzawa T. Cerium-activated Gd_2SiO_5 single crystal scintillator. Applied Physics Letters. 1983;**42**:43-45. DOI: 10.1063/1.93760

[54] International Centre for Diffraction Data [Internet]. 2019. Available from: http://www.icdd.com [Accessed: 01 August 2019]

[55] Vieira JM, Silva RA, Silva RF, Costa FM. Enhancement of superconductivity in LFZ-grown BSCCO fibres by steeper axial temperature gradients. Applied Surface

Science. 2012;**258**:9175-9180. DOI: 10.1016/j.apsusc.2011.11.054

[56] Blasse G, Grabmaier BC. Luminescent Materials. Berlin: Wiley; 1994. DOI: 10.1007/978-3-642-79017-1

[57] Lushchik A, Lushchik C, Nagirnyi V, Pazylbek S, Sidletskiy O, Schwartz K, et al. On the mechanism of radiation damage and prospects of their suppression in complex metal oxides. Physica Status Solidi B: Basic Solid State Physics. 2013;**250**:261-270. DOI: 10.1002/pssb.201200488

[58] Lushchik A, Nagirnyi V, Shablonin E, Sidletskiy O, Toxanbayev B, Zhunusbekov A. Luminescence of Cations Excitons in Gd_2SiO_5 Crystals [Internet]. Available from: http://photon-science.desy.de/annual_report/files/2009/2009545.pdf [Accessed: 01 August 2017]

[59] Kervalishvili J, Yannakopoulos PH. Nuclear Radiation Nanosensors and Nanosensory Systems. Dordrecht: Springer; 2016. DOI: 10.1007/978-94-017-7468

[60] Lee S, Lee MS, Won JY, Lee JS. Performance of a new accelerating-electrode-equipped fast-time-response PMT coupled with fast LGSO. Physics in Medicine and Biology. 2018;**63**:05NT03. DOI: 10.1088/1361-6560/aaad20

[61] Loutts GB, Zagumennyi AI, Lavrishchev SV, Zavartsev YD, Studenikin PA. Czochralski growth and characterization of $(Lu_{1-x}Gd_x)_2SiO_5$ single crystals for scintillators. Journal of Crystal Growth. 1997;**174**:331-336. DOI: 10.1016/S0022-0248(96)01171-2

[62] Zorenko Y, Gorbenko V, Savchyn V, Zorenko T, Grinyov B, Sidletskiy O, et al. Growth and luminescent properties of Ce and Ce-Tb doped $(Y,Lu,Gd)_2SiO_5$:Ce single crystalline films. Journal of Crystal Growth. 2014;**401**:577-583. DOI: 10.1016/j.jcrysgro.2014.01.066

[63] Ryba-Romanowski W, Macalik B, Berkowski M. Down- and up-conversion of femtosecond light pulse excitation into visible luminescence in cerium-doped Lu_2SiO_5-Gd_2SiO_5 solid solution crystals co-doped with Sm^{3+} or Dy^{3+}. Optics Express. 2015;**23**:4552-4562. DOI: 10.1364/OE.23.004552

[64] Kumar R, Jordan E, Gell M, Roth J, Jiang C, Wang J, et al. CMAS behavior of yttrium aluminum garnet (YAG) and yttria-stabilized zirconia (YSZ) thermal barrier coatings. Surface and Coating Technology. 2017;**327**:126-138. DOI: 10.1016/j.surfcoat.2017.08.023

[65] Guarino S, Ponticelli GS, Giannini O, Genna S, Trovalusci F. Laser milling of yttria-stabilized zirconia by using a Q-switched Yb:YAG fiber laser: Experimental analysis. International Journal of Advanced Manufacturing Technology. 2018;**94**:1373-1385. DOI: 10.1007/s00170-017-1020-8

[66] Mun JH, Jouini A, Yoshikawa A, Kim JH, Fukuda T, Lee JS. Thermal and optical properties of Yb-doped Lu_2O_3 single crystal grown by the micro-pulling-down method. Journal of Ceramic Processing Research. 2013;**14**:636-640. Available from: http://jcpr.kbs-lab.co.kr/file/JCPR_vol.14_2013/JCPR14-5/10.pdf [Accessed: 01 August 2017]

[67] Zorenko Y, Gorbenko V, Savchyn V, Voznyak T, Grinyov B, Sidletskiy O, et al. Growth and luminescent properties of Lu_2SiO_5:Ce and $(Lu_{1-x}Gd_x)_2SiO_5$:Ce single crystalline films. Journal of Crystal Growth. 2011;**337**:72-80. DOI: 10.1016/j.jcrysgro.2011.10.003

[68] Farhi H, Lebbou K, Belkahla S, Grosvalet L, Hautefeuille B, Caramanian A, et al. Fiber single crystal

growth by LHPG technique and optical characterization of Ce^{3+}-doped Lu_2SiO_5. Optical Materials. 2008;**30**:1461-1467. DOI: 10.1016/j.optmat.2007.09.002

[69] Peak JD, Melcher CL, Rack PD. Combinatorial thin film synthesis of cerium doped scintillation materials in the lutetium oxide-silicon oxide system. IEEE Transactions on Nuclear Science. 2008;**55**:1480-1483. DOI: 10.1109/TNS.2008.922839

[70] Carvalho RG, Oliveira FJ, Silva RF, Costa FM. Mechanical behaviour of zirconia-mullite directionally solidified eutectics. Materials and Design. 2014;**61**:211-216. DOI: 10.1016/j.matdes.2014.04.050

[71] Carvalho RG, Kovalevsky AV, Lufaso MW, Silva RF, Costa FM, Figueiredo FM. Ionic conductivity of directionally solidified zirconia-mullite eutectics. Solid State Ionics. 2014;**256**:45-51. DOI: 10.1016/j.ssi.2013.12.033

[72] Masubuchi Y, Higuchi M, Kodaira K. Reinvestigation of phase relations around the oxyapatite phase in the Nd_2O_3•SiO_2 system. Journal of Crystal Growth. 2003;**247**:207-212. DOI: 10.1016/S0022-0248(02)01908-5

[73] Saal JE. Thermodynamic modelling of the reactive sintering of Nd:YAG [thesis]. Pennsylvania (PA) USA: Pennsylvania State University; 2008

[74] Jiang C, Wu S, Ma Q, Mei Y. Synthesis and microwave dielectric properties of Nd_2SiO_5 ceramics. Journal of Alloys and Compounds. 2012;**544**:141-144. DOI: 10.1016/j.jallcom.2012.07.076

[75] León-Reina L, Porras-Vázquez JM, Losilla ER, Moreno-Leal L, Aranda MAG. Structure and oxide anion conductivity in $Ln_2(TO_4)O$ (Ln = La, Nd; T= Ge, Si). Journal of Solid State Chemistry. 2008;**181**:2501-2506. DOI: 10.1016/j.jssc.2008.06.029

[76] Ferreira NM, Kovalevsky AV, Costa FM, Frade JR. Processing effects on properties of $(Fe,Mg,Al)_3O_4$ Spinels as potential consumable anodes for pyroelectrolysis. Journal of the American Ceramic Society. 2016;**99**:1889-1893. DOI: 10.1111/jace.14190

[77] Nakayama S, Sakamoto M, Higuchi M, Kodaira K, Sato M, Kakita S, et al. Oxide ionic conductivity of apatite type $Nd_{9.33}(SiO_4)_6O_2$ single crystal. Journal of the European Ceramic Society. 1999;**19**:507-510. DOI: 10.1016/S0955-2219(98)00215-5